Contrib Mineral Petrol (2002) 143: 1–18
DOI 10.1007/s00410-001-0329-2

Yasuhiko Ohara · Robert J. Stern · Teruaki Ishii
Hisayoshi Yurimoto · Toshitsugu Yamazaki

Peridotites from the Mariana Trough: first look at the mantle beneath an active back-arc basin

Received: 27 April 2001 / Accepted: 10 October 2001 / Published online: 11 December 2001

Abstract Two dives of the DSV *Shinkai 6500* in the Mariana Trough back-arc basin in the western Pacific sampled back-arc basin mantle exposures. Reports of peridotite exposures in back-arc basin setting are very limited and the lack of samples has hindered our understanding of this important aspect of lithospheric evolution. The Mariana Trough is a slow-spreading ridge, and ultramafic exposures with associated gabbro dykes or sills are located within a segment boundary. Petrological data suggest that the Mariana Trough peridotites are moderately depleted residues after partial melting of the upper mantle. Although some peridotite samples are affected by small-scale metasomatism, there is no evidence of pervasive post-melting metasomatism or melt–mantle interaction. Spinel compositions plot in the field for abyssal peridotites. Clinopyroxenes show depletions in Ti, Zr, and REE that are intermediate between those documented for peridotites from the Vulcan and Bouvet fracture zones (the American–Antarctic and Southwest Indian ridges, respectively). The open-system melting model indicates that the Mariana Trough peridotite compositions roughly correspond to theoretical residual compositions after ~7% near-fractional melting of a depleted MORB-type upper mantle with only little melt or fluid/mantle interactions. The low degree of melting is consistent with a low magma budget, resulting in ultramafic exposure. We infer that the mantle flow beneath the Mariana Trough Central Graben is episodic, resulting in varying magma supply rate at spreading segments.

Y. Ohara (✉)
Ocean Research Laboratory,
Hydrographic Department of Japan,
Tokyo 104-0045, Japan
E-mail: ohara@cue.jhd.go.jp
Tel.: +81-3-35414387
Fax: +81-3-35413870

R.J. Stern
Department of Geosciences,
University of Texas at Dallas,
Richardson, TX 75083-0688, USA

T. Ishii
Ocean Research Institute,
University of Tokyo,
Tokyo 164-8639, Japan

H. Yurimoto
Department of Earth Sciences,
Tokyo Institute of Technology,
Tokyo 152-8551, Japan

T. Yamazaki
Institute for Marine Resources and Environment,
National Institute of Advanced Industrial Science
and Technology, Tsukuba 305-8567, Japan

Present address: Y. Ohara
Department of Geology and Geophysics,
Woods Hole Oceanographic Institution,
Woods Hole, MA 02543-1539, USA

Editorial responsibility: T.L. Grove

Introduction

The Philippine Sea occupies a large part of the Western Pacific, and is composed of several large back-arc basins. The Pacific Plate subducts beneath the Philippine Sea Plate along the Izu–Ogasawara–Mariana Trench (Fig. 1a). This region evolved through several episodes of arc formation, rifting and back-arc spreading (Karig 1971). The Kyushu-Palau Ridge and West Mariana Ridge are remnant arcs separated by the Parece Vela Basin. The active arc is separated from the West Mariana Ridge by an active back-arc basin, the Mariana Trough (Fig. 1a, b). The Mariana Trough is a slow-spreading back-arc basin (Fryer 1995) that is propagating northward through the Mariana arc system (Martinez et al. 1995). This is a back-arc basin where the composition and evolution of basaltic lavas have been studied extensively (Hart et al. 1972; Hawkins and Melchior 1985; Sinton and Fryer 1987; Volpe et al. 1987, 1990; Hawkins et al. 1990; Stern et al. 1990; Stolper and Newman 1994; Gribble et al. 1996, 1998).

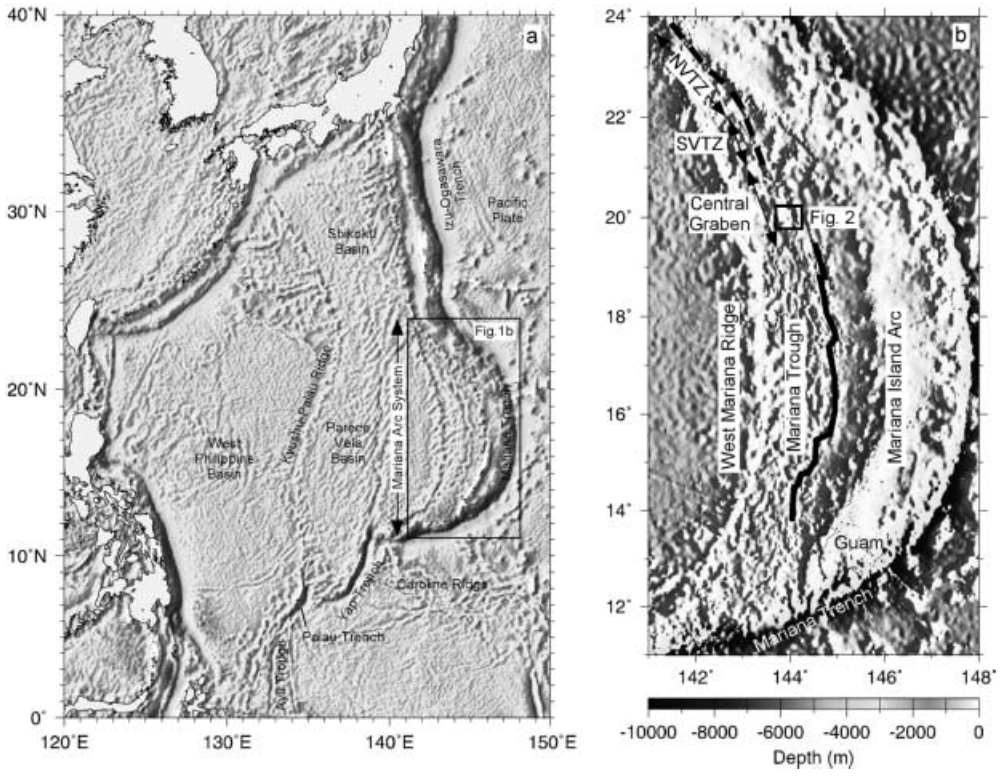

Fig. 1. **a** Satellite altimetry map showing the tectonic feature of the Philippine Sea (data from Sandwell and Smith 1997). The *rectangle* shows the location of **b**. **b** *Shaded* structural image of the Mariana arc system illuminated from 90° (data from the predicted bathymetry of Smith and Sandwell 1997). *Heavy dashed line* indicates NVTZ (northern volcano tectonic zone) and SVTZ (southern volcano tectonic zone), and *heavy plain line* indicates spreading section of the Mariana Trough. Amagmatic rifting occurs in the Central Graben. The *rectangle* shows the location of Fig. 2

Reports of peridotite exposures in back-arc basins are limited to the Mariana Trough (Bloomer et al. 1995; Stern et al. 1996, 1997) and the Parece Vela Basin (Ohara et al. 1996). Of these, only the Mariana Trough is presently active. One dredge haul during the 1991 Tunes 7 expedition aboard the R/V *Thomas Washington* first recovered back-arc basin mantle rocks (Stern et al. 1996). Two dives of the DSV *Shinkai 6500* in 1996 mapped and sampled exposures of back-arc basin mantle in the Mariana Trough (Stern et al. 1997). Stern et al. (1996) argued by analogy with mid-ocean ridges (Mutter and Karson 1992; Tucholke et al. 1998) that slow back-arc extension may be accomplished amagmatically. Although amagmatic tectonics may be common in certain phases of back-arc basin evolution based on the recent mapping study of the Philippine Sea (Ohara et al. 2001), little is known at present about the importance of this process.

In this paper, we describe in detail, for the first time, the petrology of upper mantle peridotite from the Mariana Trough, and use petrographic, mineral chemical, and ion microprobe trace element compositions to understand how these formed. In addition to the application of this information in understanding back-arc basin lithosphere evolution, these data fill a critical hole in our understanding of ophiolites. The lack of samples of back-arc basin mantle has limited our understanding of ophiolite formation because back-arc basins are thought to be very common in the inventory of ophiolites (Bloomer et al. 1995).

Geologic background and sample location

Styles of extension vary along the strike in the Mariana Trough, which can be divided into four parts (Fig. 1b; Martinez et al. 1995; Gribble et al. 1998):

1. The northern volcano-tectonic zone (NVTZ) – characterized by asymmetric rifting accompanied by fissure eruption along normal faults and point source volcanism.
2. The southern volcano-tectonic zone (SVTZ) – characterized by localization of volcanic and tectonic activity and southward-progressive separation of the extension axis from the arc.
3. The Central Graben – deeps produced by mechanical extension that expose back-arc basin lower crust and upper mantle (Stern et al. 1996).
4. South of 19.7°N – extension occurs by slow seafloor spreading. The basin is widest at 18°N, where full-spreading rates are between 3 and 4.4 cm/year (Hussong and Uyeda 1981), corresponding to those of slow-spreading mid-oceanic ridges.

These variations mark different stages in the evolution of the back-arc basin because of northward-propagating rifting and spreading. Martinez et al. (1995) argued that true seafloor spreading exists only south of 19.7°N, although Yamazaki et al. (1993) argued that spreading occurs as far north as 22°N based on magnetic data. Rifting occurs in the NVTZ, the SVTZ, and the Central Graben (Martinez et al. 1995; Baker et al. 1996).

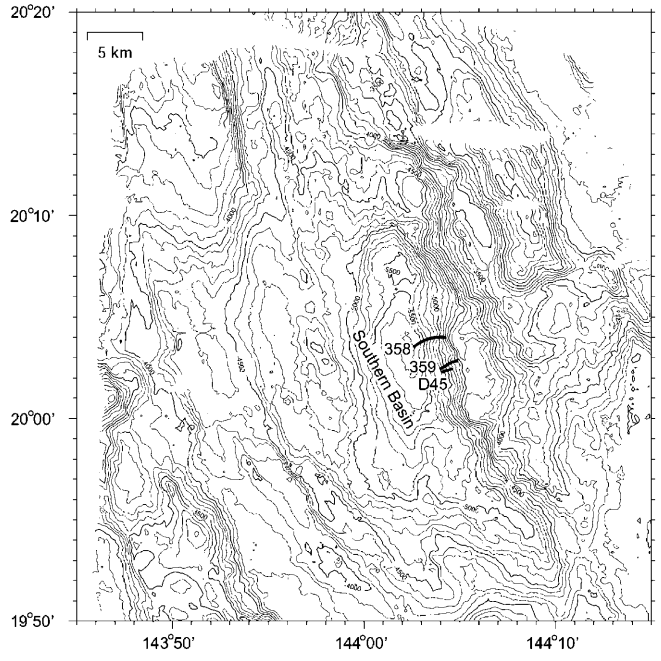

Fig. 2. Bathymetry of the Southern Graben and track lines of DSV *Shinkai 6500* dives 358 and 359. D45 represents the approximate line of the Tunes 7 dredge 45 by R/V *Thomas Washington* (Stern et al. 1996). Contours in 100-m intervals

In the Central Graben, individual grabens are located within a 20–30-km-wide sinuous bathymetric low between 21° and 19.7°N (Fig. 1b; Stern et al. 1996). The Central Graben is well delineated in the free-air gravity anomalies as a band of relative lows between about 0 and 25 mgal. Free-air gravity anomalies from distinct sub-lows within this band and reflect the bathymetric sub-basins (Martinez et al. 1995). Individual grabens are separated by along-strike bathymetric highs. Seismic lines crossing the grabens (Yamazaki et al. 1993) show that they are fault bounded, relatively sediment free, generally asymmetric, and lack evidence of active volcanism. However, recent geophysical mapping of the northern Mariana Trough suggests that a neovolcanic zone may exist in parts of the Central Graben (Yamazaki and Stern 1997). The overall structure of the Central Graben is a complex graben that is composed of four asymmetric deeps. The southernmost of these deeps (between 20°10′N and 19°50′N) is a down-to-the east half-graben (Fig. 2; "Southern Basin"; Stern et al. 1997). The Southern Basin contains the deepest point in the Mariana Trough (~5,700 m), and is remarkably deep even compared with the anomalously deep 3.6-km mean depth of the Mariana Trough back-arc basin spreading axis (Stern et al. 1996).

A single dredge in the Southern Basin was performed during the 1991 Tunes 7 expedition aboard the R/V *Thomas Washington*. The dredge (Fig. 2; D45; 20°02.5′N, 144°04.0′E; 5,175–4,800 m depth) recovered a diverse suite of upper mantle and crustal rocks, including peridotites, gabbros, and felsic plutonic rocks. The petrologic data for the Central Graben crustal suite is clearly more similar to MORB or back-arc basin crust than it is to arc crust (Stern et al. 1996). The isotopic data for D45 crustal samples are also indistinguishable from basalts from portions of the Mariana Trough undergoing seafloor spreading and distinct from those of the Mariana arc. Stern et al. (1996) concluded that the dredge recovered samples from a talus pile at the base of the eastern scarp of the Central Graben, and argued that the Southern Basin exposes a back-arc basin crustal and upper mantle section, with the crustal suite remarkably heterogeneous with gabbros, basalts, and felsic plutonic rocks.

The DSV *Shinkai 6500* dives 358 and 359 were conducted in 1996 in the Southern Basin in order to understand this unique upper mantle section (Fig. 2). Dive 358 recovered 14 samples from five sites, including gabbros, basalts, tonalite, and serpentinites. This dive is inferred to have sampled debris flows that originated from higher up the scarp (Fig. 3; Stern et al. 1997). In contrast, dive 359 traversed mountainous outcrops and steep exposures. Twenty-four samples recovered from six sites along the dive 359 track represent an upper mantle suite of 14 peridotites and 10 gabbros, inferred as younger dikes or sills (Table 1; Fig. 3; Stern et al. 1997). There is no significant Mn coating on any of these samples, suggesting these surfaces have not been exposed for very long. In addition, the presence of talus blocks observed during

Fig. 3. Schematic bathymetric profile of the east wall of the Southern Basin, the Central Graben of the Mariana Trough, with inferred subsurface lithologies (modified after Stern et al. 1997). No vertical exaggeration. Approximate positions of peridotite and gabbro samples recovered during dive 359 are shown (*S* denotes the station number). Stern et al. (1997) inferred that the petrologic Moho (the shallowest occurrence of mantle peridotites) may be exposed at a water depth about 4 km

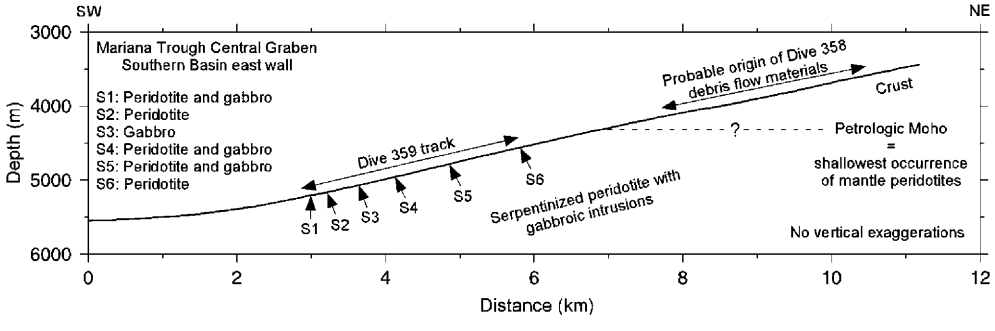

the DSV *Shinkai 6500* dive 358 suggests that most material has been reworked during tectonic events. Dive 359 documented several narrow, sediment-covered benches, suggesting that faulting is accomplished by a series of parallel, down-dropped blocks that had been displaced along steeply west-dipping normal faults (Stern et al. 1997). The eastern wall of the Southern Basin exposes a cross section of back-arc basin crust and upper mantle, with mantle exposed at depths of greater than 4,530 m along the track of dive 359 (Table 1; Figs. 2 and 3; Stern et al. 1997).

Table 1. List of the studied samples from the DSV *Shinkai 6500* dives 358 and 359

Dive	Station	Depth (m)	Sample	Remarks
358	1	5,603	358R1-1	Gabbro
	2	5,560		No sample for this study
	3	5,430		No sample for this study
	4	5,162	358R4-4	Serpentinite
	5	4,790	358R5-2	Serpentinite
359	1	5,200	359R1-1	Gabbro/peridotite boundary
			359R1-2	Peridotite
			359R1-3	Gabbro
			359R1-4	Gabbro
	2	5,149	359R2-1	Peridotite
			359R2-2	Peridotite (impregnated)
			359R2-3	Peridotite
	3	5,061	359R3-3	Peridotite
	4	4,957	359R4-2	Peridotite (impregnated)
			359R4-3	Peridotite
			359R4-4	Peridotite (impregnated)
	5	4,793	359R5-3	Peridotite
			359R5-5	Peridotite (impregnated)
	6	4,536	359R6-1	Peridotite
			359R6-2	Peridotite
			359R6-3	Peridotite

Stern et al. (1997) argue that the oceanic Moho may not mark a sharp boundary between peridotite below and mafic rocks above, as inferred from seismic refraction studies, but that the underlying mantle peridotite contains abundant mafic intrusions. These intrusions become more common as the Moho is approached; thus, the Moho marks the shallowest occurrence of mantle peridotites (Fig. 3). Stern et al. (1997) thus inferred the petrologic Moho on the eastern wall of the Southern Basin is exposed at a water depth of about 4 km, although additional DSV *Shinkai 6500* dives are necessary to prove this.

Petrography

Nineteen peridotite and gabbro samples taken from the dives 358 and 359 of DSV *Shinkai 6500* were used in this study. Primary modal compositions of the peridotites were determined by point counting. Because the alteration products form characteristic pseudomorphs after the primary phases, it is possible to determine the primary mineral assemblage even when no relict mineral remains. It is nevertheless difficult to obtain modal compositions for some samples because of injections of veins or extensive serpentinization. Representative primary modes of the peridotites along with the mean value from the American–Antarctic and Southwest Indian ridges peridotites (from the Vulcan and Bouvet fracture zones, respectively; Dick 1989) are listed in Table 2.

Peridotites

Serpentinized harzburgites dominate the peridotites; no dunites were recovered during dives 358 and 359. The rocks are highly serpentinized and have veins of hydrous silicates and rare carbonates. Secondary modal compo-

Table 2. Representative primary modal compositions of the Mariana Trough peridotites. *Ol* Olivine; *Opx* orthopyroxene; *Cpx* clinopyroxene; *Sp* spinel; *Pl* plagioclase. Each analysis is performed on 0.67×0.60-mm grid interval except for 359R1-2. Analysis for 359R1-2 is performed on 1×1-mm grid interval. No correction for differential volume expansion during serpentinization has been made. Mean Vulcan and Bouvet fracture zones data are from Dick (1989)

Sample	Ol	Opx	Cpx	Sp	Pl	Total	Total points counted	Lithology
(vol%)								
359R1-2	72.91	24.15	1.13	1.81	0.00	100.00	443	Harzburgite
359R2-1	75.09	18.62	5.05	1.25	0.00	100.00	1,445	Lherzolite
359R2-3	86.83	11.96	0.12	1.09	0.00	100.00	1,739	Harzburgite
359R3-3	73.82	22.86	0.98	2.34	0.00	100.00	1,627	Harzburgite
359R4-3	75.44	22.31	0.69	1.56	0.00	100.00	1,600	Harzburgite
359R6-1	85.10	12.49	1.90	0.51	0.00	100.00	1,369	Harzburgite
359R6-2	81.40	17.49	0.50	0.61	0.00	100.00	1,812	Harzburgite
359R6-3	76.01	21.52	1.29	1.18	0.00	100.00	1,701	Harzburgite
Mariana Trough mean	78.32	18.93	1.46	1.29	0.00	100.00	1,467	Harzburgite
1σ	5.37	4.68	1.55	0.60	0.00	0.00	439	
Vulcan FZ mean	71.13	20.56	7.33	0.96	0.03	100.01	–	Lherzolite
1σ	3.78	2.64	2.42	0.35	0.04	0.03	–	
Bouvet FZ mean	81.55	16.05	1.58	0.48	0.18	99.84	–	Harzburgite
1σ	4.18	3.44	1.31	0.29	0.40	4.81	–	

sitions were given by Stern et al. (1997), and the degree of serpentinization or alteration is approximately 40 to 95%. The peridotites consist of serpentinized olivine and bastitized orthopyroxenes (~10 mm) with minor clinopyroxene (~2 mm; Fig. 4a); however, some original phases are generally preserved. The primary mineral assemblages are weakly deformed (Fig. 4b) and the freshest portions of the rocks exhibit porphyloclastic textures (Fig. 4c). No peridotite mylonites were recovered from the sample suite in the Southern Basin, although peridotite mylonites are major constituents at slow-spreading ridges from the Atlantic and Indian Oceans (Jaroslow et al. 1996). Spinel is light reddish-brown and generally occurs as highly irregular shape intergrown with orthopyroxene (Fig. 4d), or with a symplectitic habit (Fig. 4e).

Four samples (359R2-2, 359R4-2, 359R4-4, and 359R5-5) show textural evidence of later melt or fluid impregnation by veins, although we cannot rule out the possibility that these veins are caused by alteration. The inferred impregnated parts contain altered plagioclase and euhedral to subhedral rounded spinel as diffuse veins, whereas irregular-shaped spinels are found in the harzburgitic host of the rock. Veins clearly cut the original porphyroclastic texture in 359R2-2 (Fig. 4f), hosting secondary amphibole rimming clinopyroxene. These petrological relationships suggest that the veins intruded the host peridotite after initial melting and deformation, and that these intruded as low temperature magmatic veins, or subsolidus, secondary, metasomatic veins.

Gabbros

Nearly half of the samples recovered during dive 359 are gabbros that are inferred to be dykes or sills intruded into the mantle peridotites (Figs. 3 and 4g). These are remarkably fresh and evolved, with abundant clinopyroxene (~5 mm) and little olivine (~2 mm; Stern et al. 1996). Another remarkable feature of Central Graben gabbros is abundant red-brown hornblende (~2 mm), which occurs both as rims on clinopyroxene and as primary phases (Fig. 4h). This is consistent with the much greater water content of back-arc basin basaltic magmas. Mariana Trough basaltic glasses contain up to 2.8 wt% H_2O (Gribble et al. 1996), much greater than the <0.2 wt% H_2O typical of MORB (Michael 1988). The Mariana Trough gabbros have coexisting clinopyroxene and plagioclase that are indistinguishable from mid-ocean ridge gabbros, and thus are best interpreted as forming in association with the Mariana Trough spreading (Stern et al. 1996).

Mineral chemistry

Mineral compositions were analyzed with a JEOL JCXA-733 electron microprobe at the Ocean Research Institute, University of Tokyo. The operating conditions were 15 kV accelerating voltage and 12 nA specimen current. A 1 μm beam size was used for all minerals except pyroxenes, which were measured using a broader beam size (10 μm) to average the compositional segregation caused by exsolution. Correction procedures are those of Bence and Albee (1968). Total Fe is assumed equal to Fe^{2+} except for spinel. Fe^{3+} content of spinel was calculated based on stoichiometry. The mineral compositions presented in this paper are averages of multiple core analyses (generally 10–20 analyses).

Olivine

Olivine is the major component of all peridotites. The olivine data are presented in Table 3. The forsterite content is relatively constant in each sample (Fo = ~90.5) except for impregnated samples, which show a lower forsterite content (Fo = 83–85). The NiO content of primary olivines ranges from 0.44 to 0.32 wt%, typical of mantle peridotites. All but the impregnated two samples (359R2-2 and 359R4-4) plot within the olivine–spinel mantle array (OSMA; Fig. 5; Arai 1994). Arai (1994) argues that OSMA is a residual peridotite array and that cumulates plot off this trend to the right.

The gabbros show lower Fo content and have a larger range (Fo = 59–75; Table 3) which is suggestive of crystal fractionation, or of slow cooling with partial re-equilibration between crystal and interstitial residual liquids.

Spinel

Nearly all of the peridotite samples analyzed contain some unaltered spinel. The spinel data are presented in Table 4. A plot of Mg/(Mg + Fe) ratio (= Mg#) vs. Cr/(Cr + Al) (= Cr#) ratio in spinel is shown in Fig. 6a. Primary spinel shows virtually constant Cr# ranging from 0.24 to 0.29, with Mg# ranging from 0.69 to 0.73. The Cr# of spinel in abyssal peridotites is a good indicator of the degree of melting (Dick and Bullen 1984), with the low Cr# spinels representing less-depleted peridotite and high Cr# spinels representing more-depleted peridotite. TiO_2 content of primary spinel is virtually zero, ranging from 0 to 0.05 wt% (Fig. 6b), which markedly contrasts the plagioclase-bearing abyssal peridotites from the equatorial Atlantic (Dick and Bullen 1984; Bonatti et al. 1993; Seyler and Bonatti 1997). Spinels in plagioclase-bearing peridotites are richer in Ti and Fe^{3+} and tend to be more Cr-rich compared with plagioclase-free peridotites from the same locality (Dick and Bullen 1984; Seyler and Bonatti 1997). Impregnated samples with Ti-rich spinel (359R2-2, 359R4-4, and 359R5-5; TiO_2 content are 0.092 to 0.212 wt%) also have Ti-rich clinopyroxene. These spinels also have higher Cr# (0.26–0.36) and lower Mg# (0.61–0.71). A positive correlation between Ti contents in spinel and

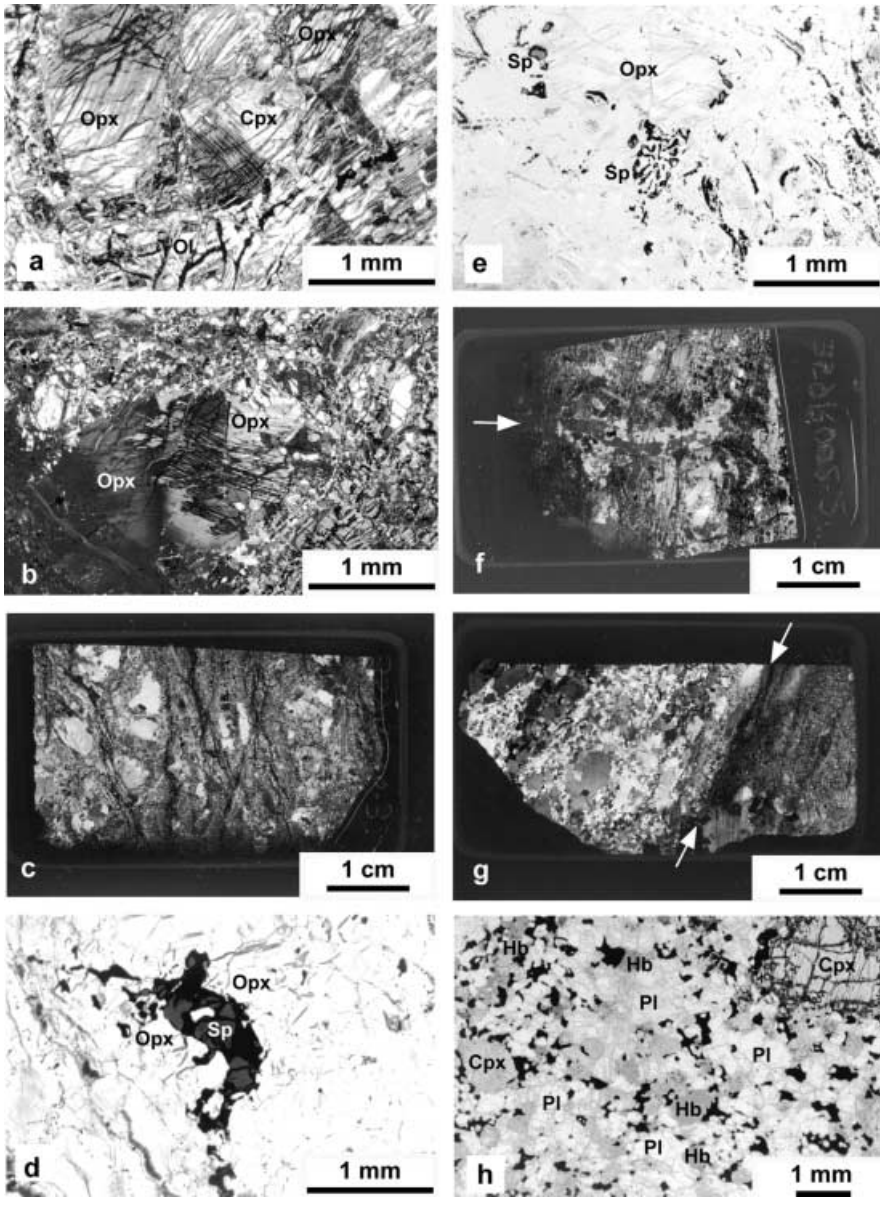

Fig. 4. **a–h** Microphotographs of thin sections and enlarged photos of thin sections, all taken with transmitted light. **a** Common habit of orthopyroxene and clinopyroxenes in the Mariana Trough peridotites. Sample 359R2-1, crossed polarizers. **b** Weakly deformed orthopyroxene in sample 359R6-3, crossed polarizers. **c** Serpentinized harzburgite with porphyloclastic texture in sample 359R6-3, crossed polarizers. **d** Irregular spinel intergrown with bastite after orthopyroxene in sample 359R2-3, plane-polarized light. **e** Symplectic spinel in sample 359R2-3, plane-polarized light. **f** Veined harzburgite. Sample 359R2-2, crossed polarizers. The vein (indicated by *white arrow*) clearly cuts the original porphyroclastic texture. **g** Contact relationships between serpentinized peridotite and gabbro. *White arrows* indicate contact boundary. Sample 359R1-1, crossed polarizers. **h** Red-brown hornblende in gabbro. Sample 359R1-3, plane-polarized light. *Ol* Olivine; *OPx* orthopyroxene; *Cpx* clinopyroxene; *Sp* spinel; *Pl* plagioclase; *Hb* hornblende

clinopyroxene is known in the abyssal peridotites (Dick and Bullen 1984; Seyler and Bonatti 1997).

Pyroxenes

Orthopyroxene and clinopyroxene compositions (Tables 5 and 6) are approximately constant, mostly falling in the enstatite and the diopside fields, respectively. Figure 7a–c shows Mg# vs. Al_2O_3, Cr_2O_3, and TiO_2 in orthopyroxene, respectively. The Mg# of primary orthopyroxene ranges from 0.90 to 0.91. The Al_2O_3 content of primary orthopyroxene ranges from 3.7 to 4.7 wt%. The orthopyroxene of impregnated sample 359R2-2 and 359R4-4 plots off the main cluster defined by the Atlantic and Indian Ocean peridotites.

Figure 8a–d shows Mg# vs. Al_2O_3, Cr_2O_3, TiO_2, and Na_2O in clinopyroxene, respectively. The Mg# of primary clinopyroxene ranges from 0.91 to 0.92, and the Al_2O_3 content varies from 4.9 to 5.5 wt%. The Cr_2O_3, TiO_2, and Na_2O contents of primary clinopyroxene are variable; Cr_2O_3 content ranges from 1.0 to 1.4 wt%, TiO_2 content from 0.09 to 0.17 wt%, and Na_2O content from 0.05 to 0.27 wt%. Al_2O_3 and Cr_2O_3 levels of Mariana Trough peridotites lie approximately midway between the least and most depleted abyssal peridotites. Na_2O and TiO_2 contents in Mariana Trough peridotites are near the most depleted compositions of abyssal peridotites overall. The clinopyroxene of impregnated samples (359R2-2, 359R4-4, and 359R5-5) plot off the main cluster defined by the Atlantic and Indian Ocean peridotites.

Table 3. EPMA analyses of olivine in the Mariana Trough peridotites and gabbros (wt%). *No. anal.* Number of analyses making up the average composition. *Fo* forsterite content. Olivine in 359R4-4 and 359R1-1 retains two different disequilibrium compositions (denoted as *a* and *b*)

Sample	Peridotite									Gabbro	
No. anal.	359R1-2 26	359R2-1 10	359R2-2 16	359R2-3 34	359R3-3 17	359R4-3 41	359R4-4a 14	359R4-4b 4	359R6-3 47	359R1-1a 15	359R1-1b 20
SiO_2	39.99	40.55	38.76	40.74	40.31	40.43	39.76	38.36	40.80	37.48	35.38
TiO_2	0.00	0.01	0.00	0.00	0.00	0.00	0.00	0.00	0.00	0.00	0.00
Al_2O_3	0.08	0.01	0.02	0.02	0.02	0.02	0.01	0.01	0.02	0.04	0.04
FeO	9.28	9.11	15.75	9.07	9.52	9.09	14.66	21.83	9.17	22.79	34.98
MnO	0.13	0.15	0.26	0.17	0.13	0.17	0.23	0.41	0.17	0.41	0.74
MgO	49.96	49.96	44.23	50.04	49.49	49.81	45.44	39.78	50.05	38.20	27.93
CaO	0.04	0.02	0.04	0.04	0.03	0.03	0.03	0.03	0.02	0.05	0.09
NiO	0.35	0.41	0.23	0.42	0.32	0.44	0.36	0.20	0.41	0.22	0.08
Total	99.83	100.22	99.28	100.49	99.81	100.00	100.50	100.62	100.65	99.18	99.24
Fo	90.6	90.7	83.4	90.8	90.3	90.7	84.7	76.5	90.7	74.9	58.7
1 (Fo)	0.2	0.2	0.3	0.1	0.2	0.2	0.3	0.2	0.2	0.3	0.2
Remarks			Impregnated				Impregnated	Impregnated			

The Mg# of gabbroic orthopyroxene ranges from 0.69 to 0.70, and the Al_2O_3 content from 1.1 to 1.2 wt%. The Mg# of gabbroic clinopyroxene ranges from 0.71 to 0.75, and the Al_2O_3 content from 1.8 to 2.3 wt%. These data again show the distinctly fractionated nature of the gabbroic pyroxenes.

Plagioclase

Plagioclase in the impregnated peridotite samples is totally altered and thus we cannot know the original compositions. Compositions of plagioclase in the gabbros are presented in Table 7. These plagioclase have a constant anorthite (An = 49–54), which, again, is quite fractionated.

REE and trace elements in clinopyroxenes

Selected peridotite clinopyroxenes were analyzed in-situ for REEs, Zr, and Ti using a Cameca IMS-3f ion microprobe both at the Tokyo Institute of Technology and the Woods Hole Oceanographic Institution. Analytical procedures at the Tokyo Institute of Technology are described by Yurimoto et al. (1989), and Wan and Yurimoto (1993), and at the Woods Hole Oceanographic Institution are described by Shimizu et al. (1978) and Johnson et al. (1990). Four clinopyroxenes from peridotite tectonites taken at stations 1, 2, 4, and 6 were analyzed, along with two clinopyroxene from impregnated samples collected at stations 2 and 4 (Fig. 3 and Table 8). Clinopyroxenes in the impregnated samples 359R2-2 and 359R4-4 lie within the host peridotite, not within the veins.

Chondrite-normalized REE patterns for clinopyroxenes are shown in Fig. 9a. Clinopyroxenes exhibit LREE-depleted REE patterns with the notable exception of the impregnated sample 359R2-2. These LREE-depleted REE patterns are similar to those reported by Johnson et al. (1990), Sobolev and Shimizu (1992, 1993) and Ross and Elthon (1997) for clinopyroxenes from abyssal peridotites. Clinopyroxene from impregnated sample 359R2-2 exhibits a flat REE pattern with a negative Eu anomaly, suggesting that the equilibrium melt experienced significant plagioclase fractionation. 359R4-4 exhibits LREE inflection in the REE pattern. This U-shaped REE pattern is generally attributed to early stage of metasomatism. Zr and Ti concentrations in clinopyroxenes are plotted in Fig. 9b. It is evident that the

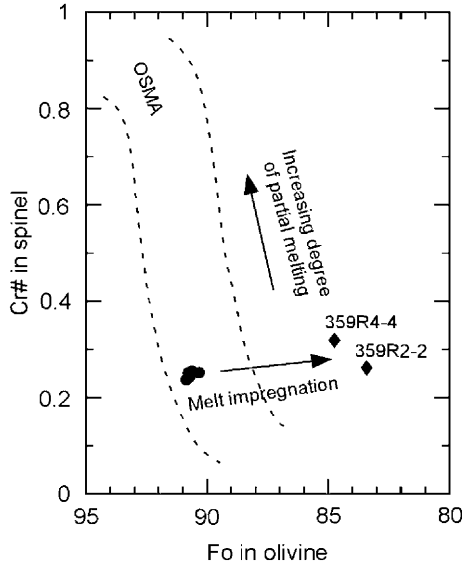

Fig. 5. Fo content of olivine vs. Cr# of coexisting spinel in Mariana Trough peridotites. Impregnated samples are shown by *filled diamonds*. The region between the *broken lines* is the olivine–spinel mantle array (OSMA), where mantle-derived spinel peridotites plot (Arai 1994). Note that impregnated samples, 359R2-2 and 359R4-4 (olivine composition is 359R4-4a; Table 3), plot off the OSMA. Olivine is absent in the other impregnated sample (359R5-5)

Table 4. EPMA analyses of spinel in the Mariana Trough peridotites (wt%). *No. anal.* Number of analyses making up the average composition

Sample	Peridotite											
No. anal.	359R1-2 19	359R2-1 2	359R2-2 22	359R2-3 15	359R3-3 10	359R4-2 18	359R4-3 14	359R4-4 21	359R5-3 15	359R5-5 20	359R6-1 10	359R6-2 6	359R6-3 40
TiO_2	0.02	0.05	0.09	0.00	0.05	0.05	0.00	0.21	0.00	0.13	0.01	0.01	0.00
Al_2O_3	45.64	46.09	43.79	46.30	46.17	42.47	46.30	39.44	43.19	36.40	42.21	43.25	45.53
FeO	11.77	13.03	13.68	11.93	12.13	12.71	11.73	16.84	13.27	13.94	12.31	13.57	12.47
Fe_2O_3	2.19	2.35	2.52	2.07	1.42	0.75	1.04	2.40	2.43	3.70	2.26	2.37	2.16
MnO	0.12	0.16	0.14	0.17	0.14	0.13	0.17	0.21	0.23	0.20	0.19	0.15	0.14
MgO	17.99	17.27	16.35	17.69	17.76	16.92	17.74	14.19	16.63	15.43	17.07	16.54	17.40
CaO	0.00	0.00	0.00	0.00	0.00	0.01	0.00	0.00	0.01	0.01	0.00	0.00	0.01
Cr_2O_3	23.09	22.02	22.91	21.81	22.77	26.78	22.43	27.23	24.73	29.91	26.04	25.06	22.68
NiO	0.25	0.26	0.23	0.29	0.23	0.15	0.25	0.25	0.25	0.26	0.25	0.25	0.26
Total	101.08	101.23	99.73	100.26	100.67	99.97	99.65	100.76	100.73	99.98	100.35	101.19	100.65
Mg#	0.732	0.704	0.683	0.725	0.725	0.705	0.729	0.606	0.691	0.667	0.712	0.685	0.713
1σ (Mg#)	0.005	0.001	0.006	0.009	0.011	0.007	0.013	0.011	0.043	0.018	0.005	0.006	0.007
Cr#	0.253	0.243	0.260	0.240	0.249	0.297	0.245	0.317	0.278	0.356	0.293	0.280	0.250
1σ (Cr#)	0.007	0.002	0.004	0.003	0.003	0.004	0.011	0.028	0.003	0.021	0.003	0.005	0.007
Remarks			Impregnated			Impregnated		Impregnated		Impregnated			

Fig. 6. a,b Spinel compositional plots, fields for abyssal peridotite are from Dick and Bullen (1984). **a** Mg# vs. Cr#. The *y* axis length is equal to two times the *x* axis, reflecting the relative molecular proportions of R^{2+} and R^{3+} cations. Impregnated samples are shown by *filled diamonds*. **b** TiO_2 wt% vs. Cr# in spinel. *Hatched area* is the range for most abyssal plagioclase-bearing peridotites (Dick and Bullen 1984). Note that impregnated samples, 359R4-4 and 359R5-5, have higher TiO_2 content

impregnated sample 359R2-2 is enriched in both Zr and Ti compared with the other peridotite clinopyroxenes.

Employing the models of Johnson et al. (1990), clinopyroxenes in the Mariana Trough peridotites (excluding 359R2-2 and 359R4-4) have residual compositions that can be explained by ~5% near-fractional melting of a depleted, MORB-type upper mantle. These observations agree with other petrological data, which indicate that Mariana Trough peridotites are moderately depleted.

Discussion

Petrological characteristics of Mariana Trough peridotites

Partial melting of the upper mantle and extraction of basaltic melts produces ultramafic tectonites as solid residues. Experimental studies indicate that progressive melting of spinel lherzolite at 10–20 kb rapidly eliminates clinopyroxene and gradually reduces the proportion of orthopyroxene (Mysen and Kushiro 1977; Jaques and Green 1980). As melting proceeds, forsterite and NiO contents of olivine, Mg# of pyroxenes, and Cr# of spinel increase, and Al_2O_3 content of spinel and pyroxenes and of the whole rock decrease. The slightly deformed porphyroclastic textures of relict primary minerals, the irregular shape of spinels, and the mineral modes of Mariana Trough peridotites further indicate an origin as residual mantle that has undergone high-temperature deformation under upper mantle plastic flow conditions. The chemistry of Mariana Trough peridotites is also compatible with a residual origin: their high contents of

Table 5. EPMA analyses of orthopyroxene in the Mariana Trough peridotites and gabbros (wt%). *No. anal.* Number of analyses making up the average composition. *En* Enstatite content; *Fs* ferrosilite content; *Wo* wollastonite content. Orthopyroxene in 359R4-4 retains two different disequilibrium compositions (denoted as *a* and *b*)

Sample	Peridotite										Gabbro	
No. anal.	359R1-2 28	359R2-1 9	359R2-2 14	359R2-3 15	359R3-3 29	359R4-3 16	359R4-4a 19	359R4-4b 10	359R5-3 19	359R6-1 10	359R6-2 7	359R6-3 42	358R1-1 30	359R1-4 49
SiO_2	53.76	55.18	52.93	54.65	54.01	54.58	54.27	54.63	54.12	54.84	53.98	55.01	52.10	53.00
TiO_2	0.04	0.02	0.03	0.02	0.04	0.01	0.08	0.07	0.02	0.00	0.05	0.02	0.39	0.32
Al_2O_3	4.45	4.20	3.86	4.26	4.65	4.53	4.37	3.49	4.68	4.20	4.00	3.73	1.20	1.08
FeO	5.97	5.88	8.83	5.94	6.14	5.87	6.84	8.85	5.71	6.00	5.80	5.81	19.50	18.96
MnO	0.13	0.21	0.19	0.17	0.13	0.17	0.16	0.20	0.17	0.16	0.09	0.17	0.67	0.66
MgO	32.22	32.85	29.79	32.60	31.96	32.49	31.91	30.95	31.49	32.90	32.15	32.51	23.76	24.33
CaO	1.89	1.47	2.35	1.31	1.74	1.42	1.59	1.60	2.23	0.79	1.88	1.76	1.34	1.36
Na_2O	0.01	0.01	0.08	0.00	0.01	0.00	0.04	0.03	0.03	0.01	0.01	0.00	0.04	0.04
Cr_2O_3	0.86	0.83	0.80	0.83	0.87	0.93	0.89	0.74	1.02	0.94	0.98	0.70	0.01	0.00
NiO	0.04	0.14	0.03	0.12	0.05	0.12	0.09	0.09	0.13	0.13	0.10	0.12	0.02	0.02
Total	99.37	100.80	98.88	99.91	99.59	100.12	100.22	100.65	99.60	99.97	99.04	99.83	99.02	99.78
Mg#	0.906	0.909	0.858	0.907	0.903	0.908	0.893	0.862	0.908	0.907	0.908	0.909	0.685	0.696
1σ (Mg#)	0.002	0.002	0.009	0.001	0.002	0.002	0.008	0.008	0.004	0.003	0.003	0.003	0.004	0.006
En	87.2	88.3	81.7	88.4	87.2	88.3	86.5	83.5	86.7	89.3	87.5	87.8	66.6	67.7
Fs	9.1	8.9	13.6	9.0	9.4	9.0	10.4	13.4	8.8	9.1	8.9	8.8	30.7	29.6
Wo	3.7	2.8	4.7	2.6	3.4	2.8	3.1	3.1	4.4	1.5	3.7	3.4	2.7	2.7
Remarks	Impregnated						Impregnated	Impregnated						

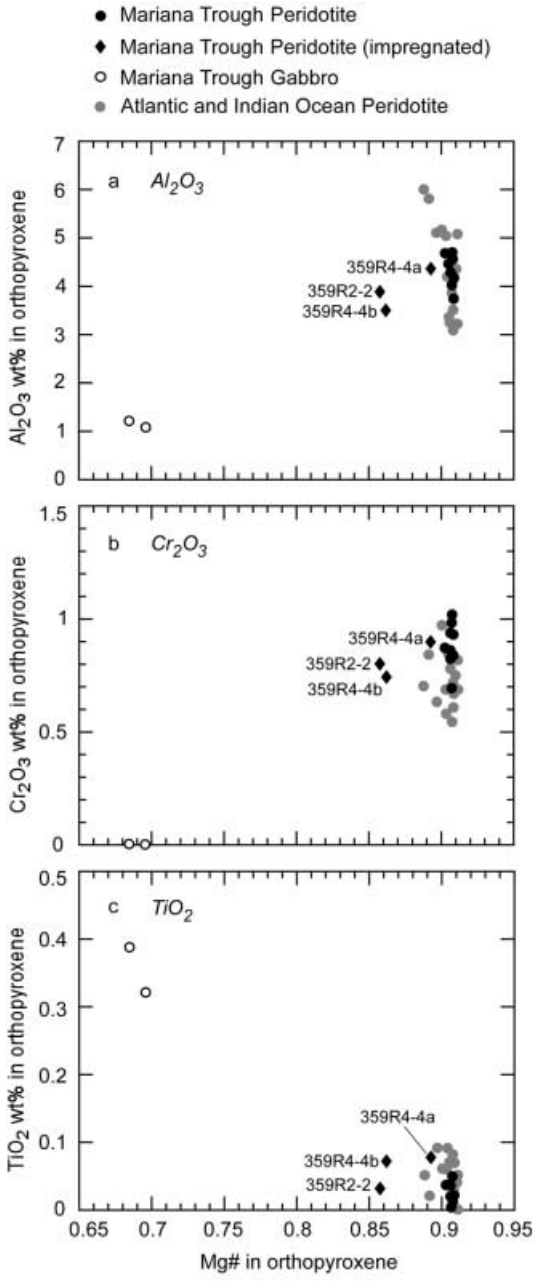

Fig. 7. Orthopyroxene compositional plots for Mariana Trough peridotites and gabbros, with fields for Atlantic and Indian Ocean peridotites for comparison (Johnson et al. 1990; Bonatti et al. 1992; Cannat et al. 1992; Johnson and Dick 1992; Cannat and Seyler 1995; Ross and Elthon 1997). **a** Mg# vs. Al_2O_3 wt%. Impregnated samples 359R2-2 and 359R4-4 plot off the main cluster defined by Atlantic and Indian Ocean peridotites. Orthopyroxene is absent in two other impregnated samples, 359R4-2 and 359R5-5. **b** Mg# vs. Cr_2O_3 wt%. **c** Mg# vs. TiO_2 wt%

compatible elements such as Ni, Cr, and Mg, and their low contents of incompatible elements such as Ti and Na.

The Marina Trough peridotites are LREE-depleted with low incompatible element abundances and have spinels with relatively low Cr# (~0.25). The moderately depleted (in terms of major elements) nature of the Mariana Trough peridotite is attested to by the modal

Table 6. EPMA analyses of clinopyroxene in the Mariana Trough peridotites and gabbros (wt%). *No. anal.* Number of analyses making 359R5-5, and 359R1-1 retains several different disequilibrium compositions (denoted as *a*, *b*, and *c*)

Sample	Peridotite							
No. anal.	359R1-2 15	359R2-1 12	359R2-2a 28	359R2-2b 11	359R2-3 6	359R4-3 6	359R4-4a 15	359R4-4b 9
SiO_2	50.18	51.59	50.99	51.53	51.22	51.05	53.37	51.83
TiO_2	0.16	0.19	0.18	0.91	0.12	0.17	0.16	0.31
Al_2O_3	5.35	5.10	3.96	2.52	4.86	5.53	3.03	3.85
FeO	2.64	2.63	3.36	5.00	2.65	2.44	3.35	4.80
MnO	0.08	0.09	0.12	0.19	0.11	0.11	0.12	0.19
MgO	16.35	16.28	16.13	16.83	16.48	16.07	16.72	15.39
CaO	23.00	23.29	22.39	21.18	23.06	23.39	23.32	22.39
Na_2O	0.08	0.27	0.47	0.43	0.11	0.20	0.36	0.50
Cr_2O_3	1.21	1.29	1.22	0.14	1.03	1.37	0.96	1.16
NiO	0.01	0.05	0.01	0.01	0.06	0.09	0.05	0.03
Total	99.07	100.78	98.83	98.74	99.70	100.40	101.45	100.45
Mg #	0.917	0.917	0.896	0.858	0.917	0.922	0.899	0.851
1σ (Mg#)	0.002	0.005	0.016	0.013	0.002	0.002	0.006	0.010
En	47.6	47.2	47.3	48.3	47.7	46.9	47.3	45.0
Fs	4.3	4.3	5.5	8.0	4.3	4.0	5.3	7.9
Wo	48.1	48.5	47.2	43.7	48.0	49.1	47.4	47.1
Remarks			Impregnated	Impregnated			Impregnated	Impregnated

compositions and the chemistry of their relict primary minerals (Mg #, Al_2O_3 and TiO_2 contents of olivine, spinel, and pyroxenes). Modal compositions of Mariana Trough peridotites are intermediate between well-characterized peridotites recovered from fracture zones on the American–Antarctic and Southwest Indian ridges (Vulcan and Bouvet fracture zones, respectively; Dick 1989; Table 2). Among the peridotites studied by Johnson et al. (1990), those from the Vulcan Fracture Zone are the least depleted and those from the Bouvet Fracture Zone are the most depleted. Compositions of spinels, orthopyroxene, and clinopyroxene in Mariana Trough peridotites consistently plot in the middle of the abyssal peridotite range (Figs. 6, 7, and 8), suggesting that the Mariana Trough peridotites are ''moderately depleted'' in a global sense.

Plagioclase is sometimes common in the abyssal peridotite samples as veins or interstitial patches (Dick and Bullen 1984; Bonatti et al. 1992; Arai and Matsukage 1996; Seyler and Bonatti 1997). These plagioclase-bearing peridotites are characterized by higher Mg/Fe ratio and enrichment in incompatible trace elements such as Ti (Dick and Bullen 1984; Seyler and Bonatti 1997), and are generally considered to be products of melt–mantle interaction (Dick and Bullen 1984; Arai and Matsukage 1996; Seyler and Bonatti 1997). No plagioclase-bearing peridotites are observed in the Mariana Trough tectonite suite, although four impregnated samples from three dive stations were found (359R2-2, 359R4-2, 359R4-4, and 359R5-5). The occurrence of impregnated peridotites that are associated with normal harzburgite and lherzolite may be caused by fractionated mafic melts intruding into peridotites that surround small and transient magma chambers beneath the Mariana Trough. The injection of fluids or melts as narrow veins (1–10 cm) in the shallow mantle could introduce Fe, Ti, LREE, and other trace elements into the peridotite (Bonatti et al. 1993). This metasomatic process could account for the ''enriched'' chemistry of spinel and pyroxenes in impregnated samples.

The overall petrological characteristics of Mariana Trough peridotites are very similar to those of peridotites drilled at the hole 920D, Ocean Drilling Program (ODP) leg 153, at the MARK area of the Mid-Atlantic Ridge, where magma channeling occurred in cold peridotites at a shallow upper mantle (Niida 1997).

Melting model

Models for magma genesis beneath mid-ocean ridges (Gast 1968), as well as recent melting experiments and observation of trace element abundances in clinopyroxenes from abyssal peridotites (Johnson et al. 1990), suggest that small volume melt fractions can be efficiently extracted from the melting mantle. Residues of such fractional melting display extremely low abundances of incompatible trace elements and extreme fractionation between those elements. Using ion microprobe analyses of clinopyroxene from abyssal peridotites from the slow-spreading ridges in the Atlantic and Indian Oceans, Johnson et al. (1990) have shown that equilibrium melting cannot produce observed trace element variations in clinopyroxene. There now is consensus that equilibrium melting of the mantle will not sufficiently deplete Zr, Ti, and REE in abyssal peridotite clinopyroxenes (Figs. 10 and 11) and also not produce liquids with Na and trace element abundances comparable with primitive MORB glasses (Johnson et al. 1990).

REE abundances in Mariana Trough peridotite clinopyroxenes are compared with those in peridotites from

up the average composition. *En* enstatite content; *Fs* ferrosilite content; *Wo* wollastonite content. Clinopyroxene in 359R2-2, 359R4-4,

				Gabbro					
359R4-4c 10	359R5-5a 21	359R5-5b 2	359R6-3 28	358R1-1 10	359R1-1a 8	359R1-1b 20	359R1-1c 9	359R1-3 79	359R1-4 46
52.17	51.51	53.89	51.38	51.03	52.01	51.45	51.69	51.89	51.96
0.88	0.12	0.02	0.09	0.66	0.57	0.57	0.62	0.53	0.53
2.53	4.59	0.99	5.33	2.27	1.95	2.03	1.98	1.95	1.84
6.43	2.77	7.43	3.15	9.85	8.45	9.26	10.30	9.02	8.93
0.27	0.11	0.39	0.14	0.38	0.25	0.33	0.33	0.37	0.37
15.90	16.11	14.00	18.53	14.41	14.54	15.03	14.12	14.54	14.72
21.10	23.12	22.80	20.01	19.81	21.25	20.16	20.03	20.88	20.72
0.44	0.16	0.60	0.05	0.46	0.39	0.38	0.39	0.44	0.43
0.19	1.46	0.73	1.21	0.01	0.07	0.00	0.01	0.00	0.00
0.03	0.06	0.02	0.09	0.03	0.01	0.01	0.02	0.02	0.03
99.94	100.00	100.87	99.97	98.89	99.49	99.22	99.48	99.65	99.53
0.815	0.912	0.770	0.913	0.723	0.754	0.743	0.710	0.742	0.746
0.012	0.011	0.015	0.005	0.012	0.006	0.010	0.014	0.012	0.011
45.9	47.0	40.5	53.4	42.2	42.1	43.3	41.2	42.0	42.5
10.4	4.5	12.1	5.1	16.2	13.7	15.0	16.8	14.6	14.5
43.7	48.5	47.4	41.5	41.7	44.2	41.7	42.0	43.4	43.0
Impregnated	Impregnated	Impregnated							

the American–Antarctic and Southwest Indian ridges (from the Vulcan and Bouvet fracture zones, respectively; Johnson et al. 1990; Figs. 9a, b). The Mariana Trough peridotite clinopyroxenes show light REE depletions similar to Bouvet, but middle and heavy REE concentrations comparable to Vulcan (Fig. 9a). The extremely depleted nature of Bouvet peridotites were attributed to extensive melting associated with plume activity at the Bouvet hot spot (Johnson et al. 1990).

Estimating the degree of melting experienced by Mariana Trough peridotites depends on assumptions of the mantle composition when melting begins, the melting mode, and partition coefficients. Based on Nd and Hf isotopic compositions of MORB, we chose a LREE-depleted lherzolite for the initial material (Table 8; Sobolev and Shimizu 1992). Partition coefficients for Ti, Zr, and REE used in the modeling are listed in Table 9. The incongruent non-modal melting mode (Table 10) is taken from Kinzler and Grove (1992). These parameters are based on anhydrous melting experiments and thus may not be appropriate for modeling melting of Mariana Trough peridotites because melting in back-arc basins is generally hydrous (Stolper and Newman 1994; Gribble et al. 1998). However, recent melting experiments, using hydrous peridotite, indicate that partition coefficients do not differ significantly between anhydrous and hydrous conditions (Gaetani et al. 1997). On this basis, we assume that the parameters are still valid for melting of Mariana Trough peridotite. The observed REE patterns of Mariana Trough clinopyroxenes can be roughly explained by ~5% near-fractional melting (Johnson et al. 1990) of depleted MORB-type upper mantle (Fig. 10; Appendix A).

Critical (continuous) melting is also possible, whereby small degrees of melting are followed by incomplete melt extraction, with some melt retained in the residue (Sobolev and Shimizu 1992, 1993). The retained melt efficiently buffers highly incompatible elements from extreme fractionation (Sobolev and Shimizu 1992, 1993). The critical melting model with ~1 wt% of retained melt at 10% melting is grossly consistent with the clinopyroxene data, although it disagrees somewhat for light REEs and heavy REEs concentrations (Fig. 10; Appendix A).

In order to better model the melting process in the Mariana Trough, we calculated the REE concentrations in Mariana Trough peridotite clinopyroxene using the open-system melting model developed by Ozawa and Shimizu (1995). The open-system melting model was first proposed by Dick et al. (1984) and refined by Johnson and Dick (1992). A quantitative model was developed by Ozawa and Shimizu (1995), in which coupling of melting and melt extraction under the influx of a LREE-enriched exotic melt or fluid is assumed. We assume that the influxed material is silicate melt in equilibrium with clinopyroxene in impregnated sample 359R2-2. This assumption may not be appropriate for inferring the melting process at depth because the influxed melt that affected sample 359R2-2 may be a shallow-level fractionate of a transient magma chamber. However, we consider that this approach utilizes the available data in the best way possible, and the results place significant constraints on mantle melting beneath the Mariana Trough.

This model reproduces the observed REE pattern of Mariana Trough peridotites with 7% melting ($F = 0.07$) of depleted mantle retaining ~0.5 wt% of interstitial melt ($\alpha = 0.005$) and a mass influx rate of 0.003 ($\beta = 0.003$) (Fig. 10; Appendix A). If infiltrating fluid is LREE-enriched, then heavy REE concentrations are primarily controlled by the degree of melting, not by the fraction of melt retained or fluid influx (Ozawa

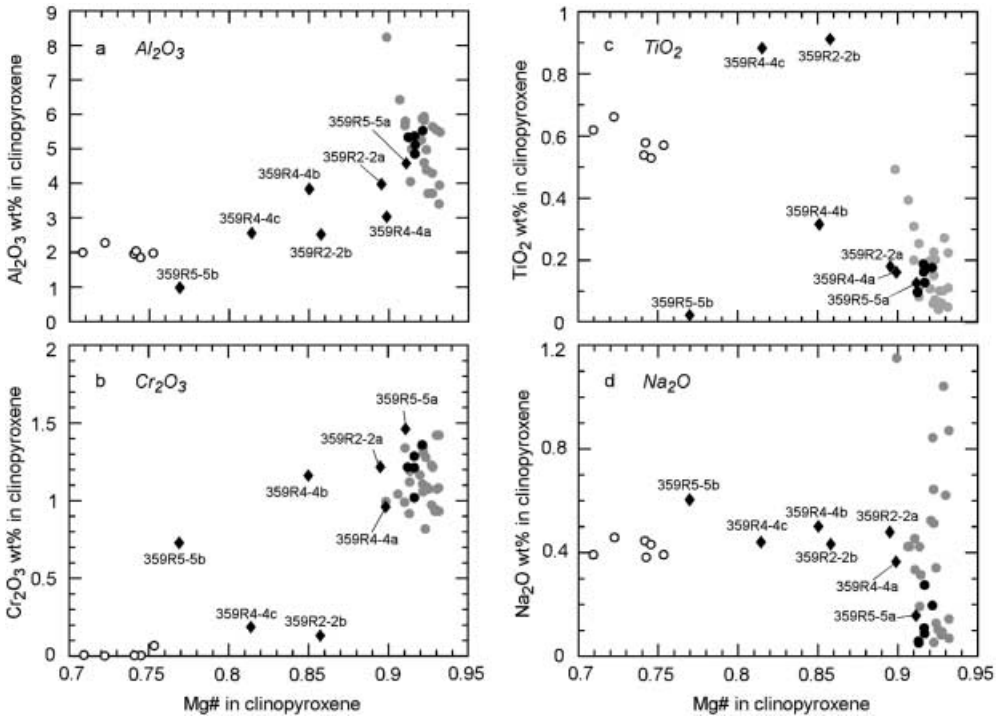

Fig. 8. a–d Clinopyroxene compositional plots for Mariana Trough peridotites and gabbros, with fields for Atlantic and Indian Ocean peridotites for comparison (Johnson et al. 1990; Bonatti et al. 1992; Cannat et al. 1992; Johnson and Dick 1992; Cannat and Seyler 1995; Ross and Elthon 1997). *Symbols* as in Fig. 7. **a** Mg# vs. Al_2O_3 wt%. Impregnated samples, 359R2-2, 359R4-4, and 359R5-5, showing wide compositional variations within the sample, are indicated. Clinopyroxene is absent in impregnated sample 359R4-2. **b** Mg# vs. Cr_2O_3 wt%. **c** Mg# vs. TiO_2 wt%. **d** Mg# vs. Na_2O wt%

Table 7. EPMA analyses of plagioclase in the Mariana Trough gabbros (wt%). *No. anal.* Number of analyses making up the average composition. *An* Anorthite content; *Ab* albite content; *Or* orthoclase content

Sample	Gabbro			
No. anal.	358R1-1 49	359R1-1 12	359R1-3 41	359R1-4 38
SiO_2	55.15	54.58	55.78	55.88
TiO_2	0.05	0.00	0.05	0.06
Al_2O_3	27.73	28.47	27.83	27.74
FeO	0.26	0.13	0.23	0.24
MnO	0.05	0.00	0.05	0.04
MgO	0.05	0.02	0.05	0.04
CaO	10.50	11.29	10.43	10.36
Na_2O	5.81	5.37	5.89	5.97
K_2O	0.09	0.05	0.07	0.07
Cr_2O_3	0.01	0.00	0.01	0.01
NiO	0.03	0.01	0.03	0.02
Total	99.73	99.94	100.41	100.44
An	49.7	53.6	49.3	48.7
Ab	49.8	46.1	50.4	50.8
Or	0.5	0.3	0.4	0.4
1σ (An)	1.4	1.0	1.5	1.1

and Shimizu 1995). Assuming a MORB-type depleted mantle source and the parameters in Tables 9 and 10, 7% melting best reproduces the observed HREE concentrations. At 7% melting, the influxed mass fraction of the initial solid is 0.021%, which is very small. Concentrations of Zr and Ti in the clinopyroxenes are consistent with both the open-system ($\alpha = 0.005$ and $\beta = 0.003$) and the critical melting model (Fig. 11). This suggests that pervasive melt or fluid–mantle interactions were insignificant for generating the Mariana Trough peridotites. This conclusion contrasts with large-scale pervasive melt–mantle interaction documented for peridotites from the East Romanche Fracture Zone, equatorial Atlantic (Seyler and Bonatti 1997) or the "refertilization" process proposed by Elthon (1992).

The clinopyroxene data show that melting in the upper mantle beneath the Mariana Trough produced melts similar to the ultra-depleted melt (in terms of incompatible trace elements) of Sobolev and Shimizu (1992, 1993). Fractional melting of the mantle led to extreme depletion, producing late-stage melts that were strongly depleted in incompatible trace elements. Depletions of high field strength elements are common in the upper mantle clinopyroxenes from beneath mid-ocean ridges (Johnson et al. 1990, 1995; Sobolev and Shimizu 1992, 1993). It appears that the production of such strongly depleted melts (in terms of incompatible trace elements) is a routine feature of magma generation beneath mid-ocean ridges and back-arc basin spreading centers.

Peridotite and basalt from the Mariana Trough

Modeling of REE, Zr, and Ti concentrations in residual clinopyroxenes indicate that most abyssal peridotites are not in equilibrium with MORB (Johnson et al. 1990; Sobolev and Shimizu 1992, 1993; Ross and Elthon 1997). Most MORBs are products of mixing between magmas, and the ultra-depleted characteristics of melts are irreversibly lost in that process (Johnson et al. 1990;

Table 8. Ion microprobe analyses of clinopyroxene in the Mariana Trough peridotites. *No. anal.* Number of analyses making up the average composition. Numbers in parentheses are standard deviations (1σ). *TITECH* Analysis at Tokyo Institute of Technology; *WHOI* analysis at Woods Hole Oceanographic Institution. Initial bulk mantle composition from Sobolev and Shimizu (1992). Chondrite composition from Anders and Ebihara (1982)

Sample No. anal.	Peridotite						Initial bulk mantle	Calculated initial clinopyroxene	Chondrite
	359R1-2 1	359R2-1 3	359R2-2 1	359R4-3 1	359R4-4 3	359R6-3 1			
(ppm)									
Ce	0.02	0.05 (0.01)	10.46	0.05	2.00 (0.24)	0.02	0.92	6.91	0.616
Pr	0.01	–	1.98	0.04	–	0.02	–		0.093
Nd	0.28	0.30 (0.02)	12.02	0.29	1.14 (0.22)	0.17	0.82	5.61	0.457
Sm	0.43	0.43 (0.02)	5.58	0.54	0.68 (0.05)	0.22	0.33	2.32	0.149
Eu	0.27	0.19 (0.04)	1.37	0.21	0.26 (0.01)	0.11	0.13	0.88	0.056
Gd	0.93	–	7.15	0.98	–	0.65	–		0.197
Tb	0.19	–	1.21	0.19	–	0.14	–		0.035
Dy	2.09	1.59 (0.09)	10.90	2.16	2.04 (0.12)	1.45	0.61	4.00	0.245
Ho	0.41	–	2.13	0.43	–	0.32	–		0.055
Er	1.69	1.02 (0.08)	6.76	1.56	1.43 (0.21)	1.20	0.40	1.89	0.160
Tm	0.17	–	0.92	0.23	–	0.16	–		0.025
Yb	1.26	0.96 (0.07)	6.57	1.40	1.34 (0.06)	1.06	0.40	2.36	0.159
Lu	0.20	–	0.81	0.20	–	0.13	–		0.024
No. anal.	1	3	1	1	3	1			
(ppm)									
Ti	983	1,259 (32)	2,707	1,075	1,092 (110)	812	1,090	4,288	436
Zr	0.5	0.9 (0.1)	69.3	1.0	2.6 (0.6)	0.3	7.5	28.1	3.9
Remarks	TITECH	WHOI	TITECH	TITECH	WHOI	TITECH			

Sobolev and Shimizu 1992). The residual mantle of Mariana Trough also is not in equilibrium with basalts from this area, nor with the intrusive gabbros.

We calculated the accumulated melt composition using the melting model tested above (equilibrium melting, fractional melting, critical melting, and open-system melting), and compared the results with spatially associated basalts from the Central Graben (Fig. 12; Appendix B; Gribble et al. 1998). As for the open-system melting model, the trace element pattern of the accumulated melt is strongly controlled by mass influx rate and less by the degree of melting (Ozawa and Shimizu 1995). Trace element concentrations in the calculated accumulated melts after the critical melting model ($\alpha = 0.01$ and $F = 0.1$) and open-system melting ($\alpha = 0.005$, $\beta = 0.003$ and $F = 0.07$) approximate the composition of the spatially associated basalts (Fig. 12), consistent with the idea that MORBs are the post-segregation accumulation of small increment melts produced during mantle melting events (Johnson et al. 1990; Sobolev and Shimizu 1992, 1993).

Basalts from along the extensional axis of the northern Mariana Trough show progressive northward changes in chemical and isotopic compositions, from typical back-arc basin basalts that formed by seafloor spreading through increasingly arc-like basalts, until volcanic rocks that are indistinguishable from arc volcanic rocks are found in the NVTZ (Gribble et al. 1998). Although we have no supporting petrological evidence such as the occurrence of primary hydrous minerals, the Mariana Trough peridotites could be the residues of hydrous mantle melting. Stolper and Newman (1994) and Gribble et al. (1996) argued that Mariana Trough basalt results from adding a water-rich "subduction component" to an N-MORB mantle source. Gribble et al. (1998) argued that Mariana Trough basalts are often – but not always – wetter than MORB. We infer that the Central Graben peridotites are the residues of low degrees of melting of a depleted MORB-type upper mantle under a relatively hydrous condition.

Tectonic implications

Ultramafic exposures on the seafloor are regarded as manifesting a low magma budget and relatively thin crust (Cannat et al. 1995). Karson et al. (1987) suggested that mantle rocks were exposed in the median valley south of the Kane Fracture Zone of the Mid-Atlantic Ridge during purely tectonic phases of spreading, without any associated igneous activity. Peridotite or gabbro exposures away from a fracture zone require thinning and stretching of the crust by low angle and listric normal faulting and by block rotations (Tucholke et al. 1998). Listric normal faulting was first suggested by Dick et al. (1981) to explain the wide range of deep crustal rocks exposed at inside corners of the Kane Fracture Zone. Exposures of mantle rocks away from fracture zones are not known along fast spreading ridges. This is because higher magma production rates and more continuous magmatic activity produce oceanic crust of more uniform and substantial thickness.

By analogy with slow spreading mid-ocean ridges, slow back-arc spreading should occasionally be amag-

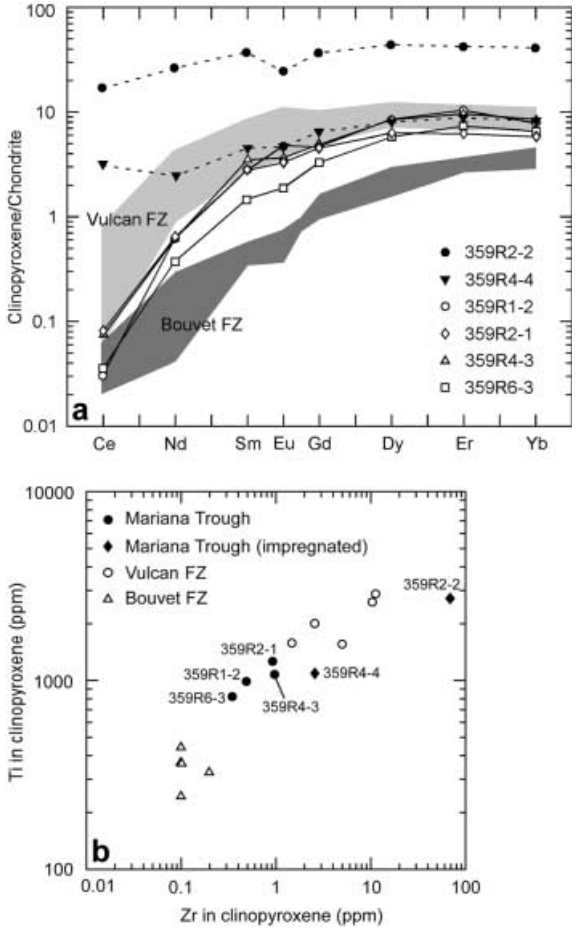

Fig. 9. a,b Ion microprobe data for clinopyroxenes from Mariana Trough peridotites (Table 8). Data for clinopyroxenes from the Vulcan and Bouvet fracture zones are shown for comparison (Johnson et al. 1990). **a** Chondrite-normalized REE patterns. Chondrite normalizing values are from Anders and Ebihara (1982). The Gd values for the samples 359R2-1 and 359R4-4 are interpolated. Impregnated samples, 359R2-2 and 359R4-4 are indicated by *dotted lines*. REE patterns of samples 359R1-2, 359R2-1, 359R4-3, and 359R6-3 have steeply sloping LREE-depleted patterns, whereas impregnated sample 359R2-2 shows rather flat REE pattern with an Eu anomaly. 359R4-4 exhibits LREE inflection in the REE pattern. The Vulcan and Bouvet data define the upper and lower limits of published REE concentrations in clinopyroxene, respectively. **b** Zr and Ti concentrations

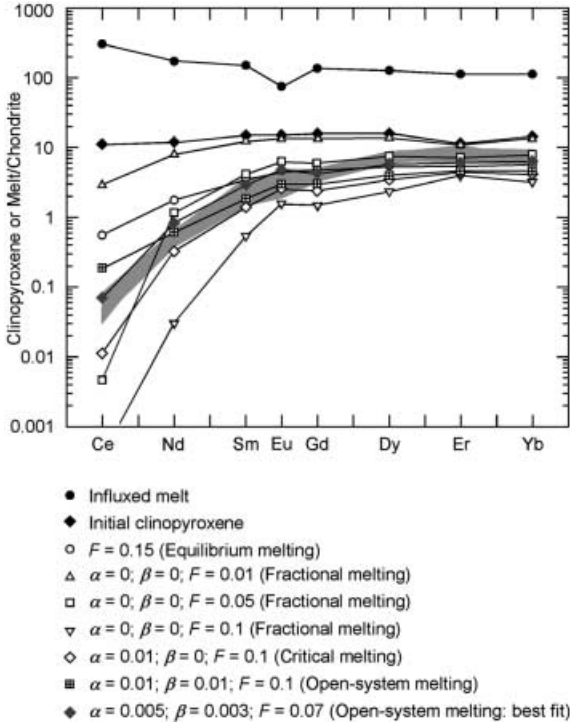

Fig. 10. REE patterns of clinopyroxene for equilibrium melting, the fractional melting, the critical melting, and the open-system melting models (Appendix A). Concentrations in influxed melt for the open-system melting model are also shown (Appendix A). The Gd values are interpolated. The model initial material is depleted MORB-type mantle (Sobolev and Shimizu 1992; Table 8) and the mineral modal composition is given in Table 10. Partition coefficients are given in Table 9, and the melting mode is after Kinzler and Grove (1992; Table 10). The range for the primary Mariana Trough peridotite data (samples 359R1-2, 359R2-1, 359R4-3, and 359R6-3) is *hatched*. The definition of the parameters is as follows (open-system melting; Ozawa and Shimizu 1995): F is degree of melting, α is mass ratio of retained melt in solid residue after the critical degree of melting is reached, and β is the mass influx rate, which is influxed mass fraction (by a LREE-enriched exotic melt or fluid) of the initial solid mass divided by degree of melting. The open-system melting model gives the solution for perfect fractional melting (Shaw 1970) by setting both α and β equal to zero, and the solution for critical melting (Sobolev and Shimizu 1993) by setting β equal to zero. The open-system melting model $\alpha = 0.005$, $\beta = 0.003$, and 7% melting ($F = 0.007$) shows good agreement with the observed Mariana Trough peridotite data. The other possible model to reproduce the Mariana Trough data is critical melting ($\alpha = 0.01$ and 10% melting)

matic. Recent bathymetric mapping of the Philippine Sea back-arc basins suggest that amagmatic tectonics is a common phenomena in certain phases of back-arc basin evolution (Ohara et al. 2001). Latest geophysical survey of the northern Mariana Trough revealed that the structure of the Central Graben is essentially the same as those of slow-spreading mid-oceanic ridges (Yamazaki et al. 1999). Yamazaki et al. (1999) argue that the Central Graben is located within a segment boundary. The location of down-to-the-east half graben along the eastern margin of the Central Graben is consistent with the presence of a west-dipping, low-angle normal fault (Stern et al. 1996, 1997). Similar structures have been documented for the earliest stages in the evolution of other back-arc basins such as the Sumisu Rift in the Izu-Ogasawara arc (Taylor et al. 1991).

The low degree of melting (~7%) estimated for the Mariana Trough peridotites is consistent with a low magma budget, resulting in ultramafic exposure in the Central Graben. Intrusive relationships between fractionated gabbro and mantle peridotite also may attest to a magma-starved spreading environment (Cannat et al. 1992). Ar–Ar dating on the hornblende of crustal gabbro-diorite dredged during the 1991 Tunes 7 expedition yields 1.8 ± 0.6 Ma (Stern et al. 1996). Based on the age data, Stern et al. (1996) argued that magmatic activity was important before 1.8 Ma, but that

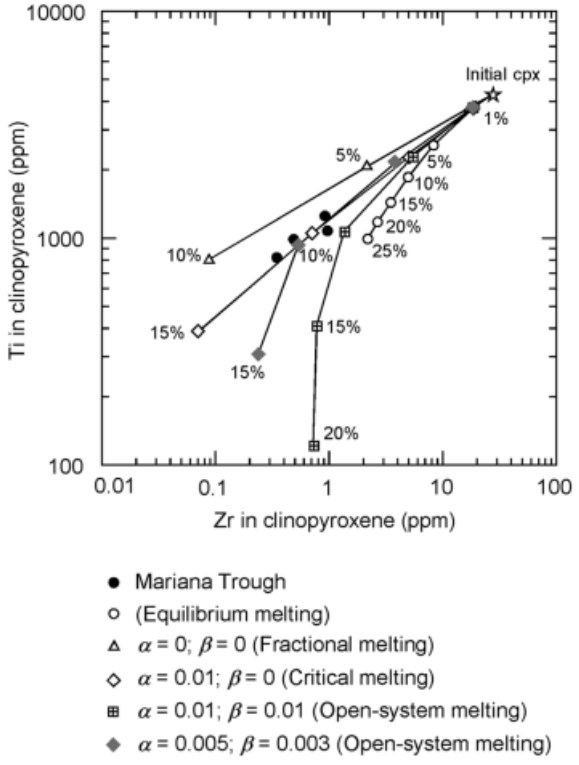

Fig. 11. Zr and Ti concentrations in modeled clinopyroxenes (Appendix B). The primary Mariana Trough peridotite data (samples 359R1-2, 359R2-1, 359R4-3, and 359R6-3) are also plotted. The open-system melting model ($\alpha = 0.005$ and $\beta = 0.003$) shows good agreement with the observed Mariana Trough peridotite data, although the critical melting model ($\alpha = 0.01$) also may account for the observed data

Table 9. Mineral/melt partition coefficients used in the models. (Data source: Sobolev and Shimizu 1992)

	Olivine	Orthopyroxene	Clinopyroxene	Spinel
Ce	0.0000	0.0006	0.0550	0.0005
Nd	0.0001	0.0090	0.1500	0.0008
Sm	0.0007	0.0100	0.2500	0.0009
Eu	0.0010	0.0192	0.3200	0.0009
Dy	0.0040	0.0210	0.3500	0.0015
Er	0.0070	0.1000	0.3700	0.0045
Yb	0.0050	0.0444	0.3700	0.0045
Ti	0.0080	0.0805	0.2300	0.1000
Zr	0.0050	0.0225	0.0750	0.0500

Table 10. Phase proportions used in the models

	Initial mode	Melting mode
Olivine	0.58	–0.30
Orthopyroxene	0.26	0.40
Clinopyroxene	0.13	0.82
Spinel	0.03	0.08

Initial mode: Sobolev and Shimizu (1992); melting mode: Kinzler and Grove (1992)

mechanical extension was more important afterwards in the Central Graben. We infer that mantle flow beneath the Central Graben is episodic, resulting in varying

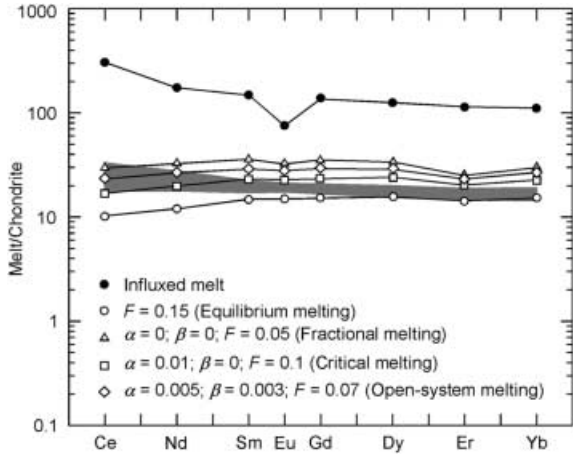

Fig. 12. REE patterns in accumulated melt for the equilibrium melting, the fractional melting, the critical melting, and the open-system melting models (Appendix A). REE patterns for Mariana Trough basalts from the Central Graben (*hatched area*; Gribble et al. 1998) are shown for comparison. Concentrations in influxed melt for the open-system melting model are also shown. The Gd values are interpolated. REE patterns in the accumulated melts using the critical melting model (Sobolev and Shimizu 1992) and open-system melting (Ozawa and Shimizu 1995) approximate the composition of the spatially associated basalts

magma supply rates beneath spreading segments. Our preferred model for the evolution of the Central Graben starts with magmatic rifting, associated with relatively "wet" BABB-type magmatism beginning about 1.8 Ma ago. Amagmatic rifting was established after 1.8 Ma. The Central Graben peridotites could be the residues of low degrees of melting of a depleted MORB-type upper mantle under relatively hydrous condition.

Conclusions

The following conclusions are drawn from the data and interpretations presented in this paper:

1. The porphyroclastic textures, modal composition, and mineral chemistry of Mariana Trough Central Graben peridotites indicate these are residual after melting.
2. Petrologic data indicate that the Central Graben peridotites are "moderately depleted" in a global sense.
3. Small-scale heterogeneity in modal compositions exists in the upper mantle beneath the Mariana Trough Central Graben, although there is no evidence for pervasive metasomatism or melt–mantle interaction.
4. Trace element compositions of clinopyroxenes in Central Graben peridotites roughly correspond to theoretical residual compositions from fractional melting of a depleted MORB-type upper mantle. Modeling of open-system melt generation suggests that 7% melting ($F = 0.07$) of a depleted source mantle with ~0.5 wt% of interstitial retained melt

($\alpha = 0.005$) at the mass influx rate 0.003 ($\beta = 0.003$) can reproduce the observed REE patterns of Central Graben peridotite clinopyroxenes.

5. Mantle exposures in the Mariana Trough Central Graben may be located within a segment boundary developed in a slow-spreading ridge. The low degree of melting (~7%) estimated for Central Graben peridotites are consistent with a low magma budget expected for a slow-spreading ridge.
6. We infer that the mantle flow beneath the Central Graben is episodic, resulting in varying magma supply rate at spreading segments. Our preferred model for the Central Graben evolution starts with magmatic rifting with relatively "wet" BABB-type magmatism before 1.8 Ma ago. After the initial magmatic rifting, amagmatic rifting occurred after 1.8 Ma.

Acknowledgements We are very grateful to the crew and scientists of the R/V *Yokosuka* and DSV *Shinkai 6500* for their professional work. We thank Kazuhito Ozawa for critical discussions on open-system melting model. We appreciate Nobumichi Shimizu for his help with the ion microprobe work at Woods Hole Oceanographic Institution. We also thank Henry Dick for fruitful discussion and encouragement. Comments from Kevin Johnson and an anonymous referee improved this paper. GMT 3.0 (Wessel and Smith 1995) was used to map bathymetric data.

Appendix A Results of the simulation (for REEs) discussed in the text

	Calculated initial clinopyroxene	Influxed melt	Modeled clinopyroxene							Accumulated melt			
			1	2	3	4	5	6	7	8	10	11	9
(Normalized)													
Ce_N	11.22	308.62	0.55	2.92	0.00	0.00	0.01	0.19	0.07	9.92	16.39	23.60	29.86
Nd_N	12.28	175.42	1.76	8.14	1.17	0.03	0.33	0.60	0.83	11.73	19.28	26.44	33.45
Sm_N	15.58	149.74	3.59	12.39	4.17	0.54	1.43	1.81	2.91	14.36	22.86	29.72	35.92
Eu_N	15.74	76.39	4.74	13.42	6.33	1.59	2.69	2.90	4.67	14.81	22.81	28.32	33.10
Gd_N	15.96	138.43	4.53	13.32	5.85	1.46	2.48	2.88	4.36	15.00	23.28	29.33	34.55
Dy_N	16.34	127.11	5.47	14.26	7.53	2.38	3.54	3.96	5.80	15.64	23.70	28.93	33.17
Er_N	11.81	114.11	5.22	10.84	7.35	3.91	4.54	4.87	6.21	14.12	20.30	23.39	25.67
Yb_N	14.85	111.60	5.65	13.29	7.94	3.25	4.24	4.59	6.37	15.28	22.65	26.93	30.28

where: *1* equilibrium melting ($F = 0.15$); *2* fractional melting ($\alpha = 0$, $\beta = 0$, $F = 0.01$); *3* fractional melting ($\alpha = 0$, $\beta = 0$, $F = 0.05$); *4* fractional melting ($\alpha = 0$, $\beta = 0$, $F = 0.1$); *5* critical melting ($\alpha = 0.01$, $\beta = 0$, $F = 0.1$); *6* open-system melting ($\alpha = 0.01$, $\beta = 0.01$, $F = 0.1$); *7* open-system melting ($\alpha = 0.005$, $\beta = 0.003$, $F = 0.07$); *8* equilibrium melting ($F = 0.15$); *9* fractional melting ($\alpha = 0$, $\beta = 0$, $F = 0.05$); *10* critical melting ($\alpha = 0.01$, $\beta = 0$, $F = 0.1$); *11* open-system melting ($\alpha = 0.005$, $\beta = 0.003$, $F = 0.07$). Influxed melt composition is calculated from the clinopyroxene composition of 359R2-2. Normalizing value from Anders and Ebihara (1982). Gd values are interpolated

Appendix B Results of the simulation (for Ti and Zr) discussed in the text

	α	β	F	Ti (ppm)	Zr (ppm)
Calculated initial clinopyroxene	–	–	–	4,287.67	28.13
Influxed melt	–	–	–	11,771.44	924.27
Equilibrium melting	–	–	0.01	3,786.67	19.22
	–	–	0.05	2,580.55	8.48
	–	–	0.10	1,845.69	4.99
	–	–	0.15	1,436.59	3.54
Fractional melting	–	–	0.20	1,175.95	2.74
	–	–	0.25	995.35	2.23
	0	0	0.01	3,746.44	17.54
	0	0	0.05	2,055.42	2.18
	0	0	0.10	804.42	0.09
Critical melting	0.01	0	0.01	3,786.66	19.22
	0.01	0	0.05	2,284.92	4.98
	0.01	0	0.10	1,062.41	0.71
	0.01	0	0.15	390.22	0.07
Open-system melting	0.01	0.01	0.01	3,785.03	19.39
	0.01	0.01	0.05	2,282.90	5.51
	0.01	0.01	0.10	1,069.66	1.40
	0.01	0.01	0.15	409.85	0.80
	0.01	0.01	0.20	120.90	0.74
Open-system melting	0.005	0.003	0.01	3,776.79	18.94
	0.005	0.003	0.05	2,181.78	3.84
	0.005	0.003	0.10	941.78	0.54
	0.005	0.003	0.15	309.89	0.24

Influxed melt composition is calculated from the clinopyroxene composition of 359R2-2.

References

Anders E, Ebihara M (1982) Solar-system abundances of the elements. Geochim Cosmochim Acta 46:2363–2380

Arai S (1994) Compositional variation of olivine–chromian spinel in Mg-rich magmas as a guide to their residual spinel peridotites. J Volcanol Geotherm Res 59:279–293

Arai S, Matsukage K (1996) Petrology of the gabbro–troctolite–peridotite complex from Hess Deep, Equatorial Pacific: implications for mantle–melt interaction within the oceanic lithosphere. In: Mével C, Gillis KM, Allan JF, Meyer PS (eds) Proceedings of the Ocean Drilling Program, Scientific Results 147, ODP, College Station, Texas, pp 135–155

Baker N, Fryer P, Martinez F, Yamazaki T (1996) Rifting history of the northern Mariana Trough: SeaMARC II and seismic reflection surveys. J Geophys Res 101:11427–11455

Bence AE, Albee AL (1968) Empirical correction factors for the electron microanalysis of silicates and oxides. J Geol 76:382–403

Bloomer SH, Taylor B, MacLeod CJ, Stern RJ, Fryer P, Hawkins J, Johnson L (1995) Early arc volcanism and ophiolite problem: a perspective from drilling in the Western Pacific. In: Taylor B, Natland J (eds) Active margins and marginal basins of the Western Pacific. Am Geophys Union Geophys Monogr 88:1–30

Bonatti E, Peyve A, Kepezhinskas P, Kurentsova N, Seyler M, Skolotnev S, Udintsev G (1992) Upper mantle heterogeneity below the Mid-Atlantic Ridge, 0–15°N. J Geophys Res 97:4461–4476

Bonatti E, Seyler M, Sushevskaya N (1993) A cold suboceanic mantle belt at the Earth's equator. Science 261:315–320

Cannat M, Seyler M (1995) Transform tectonics, metamorphic plagioclase and amphibolitization in ultramafic rocks of the Vema transform fault (Atlantic Ocean). Earth Planet Sci Lett 133:283–298

Cannat M, Bideau D, Bougault H (1992) Serpentinized peridotites and gabbros in the Mid-Atlantic Ridge axial valley at 15°37′N and 16°52′N. Earth Planet Sci Lett 109:87–106

Cannat M, Mével C, Maia M, Deplus C, Durand C, Gente P, Agrinier P, Belarouchi A, Dubuisson G, Humler E, Reynolds J (1995) Thin crust, ultramafic exposures, and rugged faulting patterns at the Mid-Atlantic Ridge (22–24°N). Geology 23:49–52

Dick HJB (1989) Abyssal peridotites, very slow spreading ridges and ocean ridge magmatism. In: Saunders AD, Norry MJ (eds) Magmatism in the ocean basins. Geol Soc Spec Publ 42:71–105

Dick HJB, Bullen T (1984) Chromian spinel as a petrogenetic indicator in abyssal and alpine-type peridotites and spatially associated lavas. Contrib Mineral Petrol 86:54–76

Dick HJB, Bryan WB, Thompson G (1981) Low angle faulting and steady state emplacement of plutonic rocks at ridge-transform intersections. EOS Trans Am Geophys Union 62:406

Dick HJB, Fisher RL, Bryan WB (1984) Mineralogic variability of the uppermost mantle along mid-ocean ridges. Earth Planet Sci Lett 69:88–106

Elthon D (1992) Chemical trends in abyssal peridotites: refertilization of depleted suboceanic mantle. J Geophys Res 97:9015–9025

Fryer P (1995) Geology of the Mariana Trough. In: Taylor B (ed) Back-arc basins: tectonics and magmatism. Plenum Press, New York, pp 237–279

Gaetani GA, Kent AJR, Grove TL, Hutcheon ID, Stolper EM (1997) Experimental determination of the partitioning of trace elements between peridotite minerals and silicate melts with variable water contents. EOS Trans Am Geophys Union 78:839–840

Gast PW (1968) Trace element fractionation and the origin of tholeiitic and alkaline magma types. Geochim Cosmochim Acta 32:1057–1086

Gribble RF, Stern RJ, Bloomer SH, Stuben D, O'Hearn T, Newman S (1996) MORB mantle and subduction components interact to generate basalts in the southern Mariana Trough back-arc basin. Geochim Cosmochim Acta 60:2153–2166

Gribble RF, Stern RJ, Newman S, Bloomer SH, O'Hearn T (1998) Chemical and isotopic composition of lavas from the northern Mariana Trough: implications for magmagenesis in back-arc basins. J Petrol 39:125–154

Hart SR, Glassley WE, Karig DE (1972) Basalts and sea floor spreading behind the Mariana Island Arc. Earth Planet Sci Lett 15:12–18

Hawkins JW, Melchior JT (1985) Petrology of Mariana Trough and Lau Basin basalts. J Geophys Res 90:11431–11468

Hawkins JW, Macdougall JD, Volpe AM (1990) Petrology of the axial ridge of the Mariana Trough back-arc spreading center. Earth Planet Sci Lett 100:226–250

Hussong DM, Uyeda S (1981) Tectonic processes and the history of the Mariana arc synthesis of the results of Deep Sea Drilling Leg 60. In: Hussong DM, Uyeda S, Blanchet R et al. (eds) Initial Reports Deep Sea Drilling Project 60, US Government Printing Office, Washington, DC, pp 909–929

Jaques AJ, Green DH (1980) Anhydrous melting of peridotite at 0–15 kb pressure and the genesis of tholeiitic basalts. Contrib Mineral Petrol 73:287–310

Jaroslow GE, Hirth G, Dick HJB (1996) Abyssal peridotite mylonites: implications for grain-size sensitive flow and strain localization in the oceanic lithosphere. Tectonophysics 256:17–37

Johnson KTM, Dick HJB (1992) Open system melting and temporal and spatial variation of peridotite and basalt at the Atlantis II Fracture Zone. J Geophys Res 97:9219–9241

Johnson KTM, Dick HJB, Shimizu N (1990) Melting in the oceanic upper mantle: an ion microprobe study of diopsides in abyssal peridotites. J Geophys Res 95:2661–2678

Johnson KTM, Fisk MR, Naslund HR (1995) Geochemical characteristics of refractory silicate melt inclusions from Leg 140 diabases. In: Erzinger J, Becker K, Dick HJB, Stokking LB (eds) Proceedings of the Ocean Drilling Program, Scientific Results 137/140, ODP, College Station, Texas, pp 131–139

Karig DE (1971) Origin and development of marginal basins in the Western Pacific. J Geophys Res 76:2542–2561

Karson JA, Thompson G, Humphris SE, Edmond JM, Bryan WB, Brown JR, Winters AT, Pockalny RA, Casey JF, Campbell AC, Klinkhammer G, Palmer MR, Kinzler RJ, Sulanowska MM (1987) Along axis variation in seafloor spreading in the MARK area. Nature 328:681–685

Kinzler RJ, Grove TL (1992) Primary magmas of mid-ocean ridge basalts. 1. Experiments and methods. J Geophys Res 97:6885–6907

Martinez F, Fryer P, Baker NA, Yamazaki T (1995) Evolution of back-arc rifting: Mariana Trough 20–24°N. J Geophys Res 100:3807–3827

Michael PJ (1988) The concentration, behavior, and storage of H_2O in the suboceanic upper mantle: implications for mantle metasomatism. Geochim Cosmochim Acta 52:555–566

Mutter JC, Karson JA (1992) Structural processes at slow-spreading ridges. Science 257:627–634

Mysen BO, Kushiro I (1977) Compositional variation of coexisting phases with degree of melting of peridotite in the upper mantle. Am Mineral 62:843–865

Niida K (1997) Mineralogy of MARK peridotites: replacement through magma channeling examined from Hole 920D, MARK area. In: Karson JA, Cannat M, Miller DJ, Elthon D (eds) Proceedings of the Ocean Drilling Project, Scientific Results 153, ODP, College Station, Texas, pp 265–275

Ohara Y, Kasuga S, Ishii T (1996) Peridotites from the Parece Vela Rift in the Philippine Sea: upper mantle material exposed in an extinct back-arc basin. Proc Jpn Acad Ser B 72:118–123

Ohara Y, Yoshida T, KatoY, Kasuga S (2001) Giant megamullion in the Parece Vela back-arc basin. Mar Geophys Res 22:47–61

Ozawa K, Shimizu N (1995) Open-system melting in the upper mantle: constraints from the Hayachine–Miyamori ophiolite, northeastern Japan. J Geophys Res 100:22315–22335

Ross K, Elthon D (1997) Extreme incompatible trace-element depletion of diopside in residual mantle from south of the Kane

Fracture Zone. In: Karson JA, Cannat M, Miller DJ, Elthon D (eds) Proceedings of the Ocean Drilling Project, Scientific Results 153, ODP, College Station, Texas, pp 277–284
Sandwell DT, Smith WHF (1997) Marine gravity anomaly from Geosat and ERS 1 Satellite altimetry. J Geophys Res 102:10039–10054
Seyler M, Bonatti E (1997) Regional-scale melt-rock interaction in lherzolitic mantle in the Romanche Fracture Zone (Atlantic Ocean). Earth Planet Sci Lett 146:273–287
Shaw DM (1970) Trace element fractionation during anatexis. Geochim Cosmochim Acta 34:137–143
Shimizu N, Semet MP, Allegre CJ (1978) Geochemical application of quantitative ion-microprobe analysis. Geochim Cosmochim Acta 42:1321–1334
Sinton JM, Fryer P (1987) Mariana Trough lavas from 18°N: implications for the origin of back arc basin basalts. J Geophys Res 92:12782–12802
Smith WHF, Sandwell DT (1997) Global seafloor topography from satellite altimetry and ship depth soundings. Science 277:1957–1962
Sobolev AV, Shimizu N (1992) Superdepleted melts and ocean mantle permeability. Doklady Rossiyskoy Akademii Nauk 326:354–360
Sobolev AV, Shimizu N (1993) Ultra-depleted primary melt included in an olivine from the Mid-Atlantic Ridge. Nature 363:151–154
Stern RJ, Lin P, Morris JD, Jackson MC, Fryer P, Bloomer SH, Ito E (1990) Enriched back-arc basin basalts from the northern Mariana Trough: implications for the magmatic evolution of back-arc basins. Earth Planet Sci Lett 100:210–225
Stern RJ, Bloomer SH, Martinez F, Yamazaki T, Harrison TM (1996) The composition of back-arc basin lower crust and upper mantle in the Mariana Trough: a first report. Island Arc 5:354–372
Stern RJ, Yamazaki T, Danishwar S, Sun C-H (1997) Back-arc basin lower crust and upper mantle in the northern Mariana Trough studied with "Shinkai 6500". Jpn Mar Sci Tech Center J Deep Sea Res 13:47–61
Stolper E, Newman S (1994) The role of water in the petrogenesis of Mariana Trough magmas. Earth Planet Sci Lett 121:293–325
Taylor B, Klaus A, Brown GR, Moore GF, Okamura Y, Murakami F (1991) Structural development of Sumisu Rift, Izu-Bonin arc. J Geophys Res 96:113–129
Tucholke B, Lin J, Kleinrock M (1998) Megamullions and mullion structure defining oceanic metamorphic core complexes on the Mid-Atlantic Ridge. J Geophys Res 103:9857–9866
Volpe AM, Macdougall JD, Hawkins JW (1987) Mariana Trough basalts (MTB): trace element and Sr–Nd isotopic evidence for mixing between MORB-like and arc-like melts. Earth Planet Sci Lett 82:241–254
Volpe AM, Macdougall JD, Lugmair GW, Hawkins JW, Lonsdale P (1990) Fine-scale isotopic variation in Mariana Trough basalts: evidence for heterogeneity and a recycled component in back-arc basin mantle. Earth Planet Sci Lett 100:251–264
Wan W, Yurimoto H (1993) Analysis of rare earth elements in garnet by SIMS. Annu Rep Geosci Univ Tsukuba 19:87–91
Wessel P, Smith WHF (1995) New version of the Generic Mapping Tools released. EOS Trans Am Geophys Union 76:329
Yamazaki T, Stern RJ (1997) Topography and magnetic vector anomalies in the Mariana Trough. Jpn Mar Sci Tech Center J Deep Sea Res 13:31–45
Yamazaki T, Murakaki F, Saito E (1993) Mode of seafloor spreading in the northern Mariana Trough. Tectonophysics 221:207–222
Yamazaki T, Okino K, Hasegawa Y, Saitake H, Ito M (1999) Geophysical mapping of Mariana Trough and West Philippine Basin: a preliminary report of *Kairei KR98-12* cruise. Jpn Mar Sci Tech Center J Deep Sea Res 15(II):63–72
Yurimoto H, Yamashita A, Nishida N, Sueno S (1989) Quantitative SIMS analysis of GSJ rock reference samples. Geochem J 23:215–236